Journal of Ovonic Research Vol. 18, No. 3, May - June 2022, p. 373 - 388

# Correlation between structural, optical, and electrical properties of sol–gel-derived ZnO thin films

A. F. Al Naim[a], A. Solieman[b], E. R. Shaaban[b,*]
[a]*Physics Department, College of Science, King Faisal University, KSA*
[b]*Physics Department, Faculty of Science, Al-Azhar University, Assiut, 71542, Egypt*

To study their structural, electrical, and optical properties, samples of Zinc oxide (ZnO) thin films were deposited from zinc acetate dehydrate (ZAD) sol of different sol concentrations prepared by using sol–gel technology and spin coating process. After deposition, the deposited thin layers were cured at different sintering temperatures. The impact of changes in sol molarity and sintering temperature on the microstructure properties of the ZnO films was studied by X-ray diffractometry (XRD). The microstructure results of grain orientation, crystallite size, lattice strain, and residual stress were measured for different sol concentrations and different sintering temperatures. From the optical measurements along wavelengths from 200 to 2200 nm, all ZnO thin films exhibited a very high transmittance (~90%) in the infrared and visible light range. At wavelengths of ultraviolet range ($\lambda \leq 400$ nm) the value of transmittance decreased sharply owing to the high value of optical gap energy of ZnO thin layers. The estimated value of optical gap energy augmented from 3.24 eV to 3.55 eV when the solution molarity raised from 0.2 to 0.8 M, respectively. For ZnO thin films of 0.4 M concentration, the band-gap energy increased with an excess in the sintering temperature. The electrical resistivity of the ZnO film decreased with an augment in sol concentration from 0.2 to 0.4 M and its value increased by increasing the sol concentration. The lowest electrical resistivity was 22.0 Ω.cm, which was achieved after sintering 0.4 M ZnO film at 550°C for 1 h followed by annealing at 500°C in forming gas for 30 min. The variation of microstructural parameters was correlated strongly with the electrical and optical properties of the ZnO thin films. The relationship between the structural, optical and electrical parameters is discussed.

(Received February 7, 2022; Accepted May 11, 2022)

*Keywords:* Sol–gel, Microstructure, Band-gap energy, Electrical resistivity, Lattice strain, Grain size

## 1. Introduction

Much attention has been driven by scientific research of ZnO thin films that is taken into consideration as a favorable substitute transparent conductive oxide. The high value of both optical band gap energy (≥ 3 eV) and exciton energy (~ 60 meV) [1.2] at room temperature is the most important property encourages researchers for studying ZnO thin films to be used as transparent conductive oxide (TCO) layers in several electro-optical applications. In addition to that, ZnO is a suitable candidate for such applications because of its nonexpensive manufacturing, non-toxicity, and highly durable against hydrogen plasma compared to ITO. Therefore, ZnO is a future attractive TCO in several optoelectronic appliances, such as laser diodes, blue/ultraviolet light-emitting diodes, UV photodetectors, and transparent thin-films transistor [3,4]. Acoustic wave and piezoelectric devices [5,6] are other promising areas of application for ZnO. Nanostructured ZnO films can be used as transparent electrodes and window layer for solar cells [7], biosensors [8], and gas sensors [9,10]. Nonetheless, many difficulties accompanying the replacing of ZnO based TCO films for ITO remain occur.

[*] Corresponding author: esam_ramadan2008@yahoo.com
https://doi.org/10.15251/JOR.2022.183.373

Many researchers have used different physical and chemical techniques to fabricate ZnO thin films. The preparation methods include thermal evaporation [11], sputtering [12], pulsed laser deposition [7], chemical vapor deposition [13], spray pyrolysis [14], metal-oxide chemical vapor deposition [15], molecular beam epitaxy [16], and the sol–gel process [17]. Despite the wide use of the physical deposition methods, the sol–gel technique has several advantages over the other techniques because of its simplicity, high compositional control, excellent molecular-level homogeneity, and inferior crystallization temperature.

ZnO thin films can be deposited in wurtzite (hcp), rock salt (fcc), cesium chloride (sc), or zinc blend (fcc) structure phases [18]. At ambient conditions, ZnO can be crystallized in polygonal structure with a wurtzite hexagonal lattice and several different preferred orientations depending on fabrication factors, such as the deposition technique, sol concentration, and heat treatment. The C-axis orientation of high-intensity (002) peak indicates the high atomic density with a free internal stress and minimum value of free surface energy. The quality of the ZnO transparent conductive layer can be controlled by its crystallinity and grain orientation, surface homogeneity, optical transmission, and electrical conductivity. The pre- and post- deposition heat treatment has significant outcome on the structural and physical characteristics of the thin coatings. The physical properties of numerous metal-oxide films, such as $TiO_2$ [19], $In_2O_3$ [20], and $SnO_2$ [21] films, are influenced by heat treatment. Many researchers [22] have described the impact of annealing conditions on the crystallite size, surface smoothness and roughness, photoluminescence, and thermo-luminescence of ZnO films. However, the crystalline phase structure, lattice dimensions and grain orientation of pure and doped ZnO films were found to be directly dependent on the heat treatment [23]. Moreover, for different kinds of thin films derived by sol-gel technique, several parameters affect the features and properties of the films, such as the molar concentration of precursor, preparation techniques (spin and dip coating), aging time, doping concentration, withdrawal speed, drying condition, number of layers, sintering temperature, and annealing conditions. The effect of most parameters has been studied and the parameters have been found to influence the quality of the ZnO thin films directly or indirectly [24-27]. The effect of heat treatment and process parameters requires an increased understanding to obtain ZnO thin films with a high quality by applying the sol–gel method. Despite the progress made, several important issues require additional understanding and resolution. Even though many studies exist on the preparation and description of sol–gel ZnO thin films, the correlation between their structural, electrical, and optical properties has not been scrutinized thoroughly. Therefore, our work helps to provide information on the correlation between the microstructure and physical properties of ZnO thin films. We fabricated ZnO coatings by sol–gel technology through spin coating process and aimed to establish the relationship between the structural, electrical, and optical properties of the ZnO thin films. The effect of sol concentration, sintering in air, and annealing in forming gas FG ($N_2/H_2$:92/08) on the microstructural properties, surface morphology, optical transparency, and electrical conductivity was studied.

## 2. Experimental

Borosilicate glass sheets with a high transparency over a wide range of wavelengths were used as substrates for ZnO thin films. The glass substrates were cut into 3 cm × 3 cm pieces. The substrates were cleaned by washing using distilled water, rinsed in ethanol, ultrasonicated for 30 min in ethanol, rinsed in distilled water, and dried using a nitrogen gas gun.

An appropriate amount of zinc-acetate dehydrate (ZAD, Sigma-Aldrich Company), was dissolved in ethanol at room temperature with magnetic stirring. By using a hot-plate with magnetic stirring and a temperature controller, the temperature of the ZAD solution was increased to 80°C with continuous stirring until a clear and homogeneous solution was obtained. An amount of di-ethanolamine was added to the solution dropwise in a 1:1 molar ratio to Zn. Solution stirring was continued at 80°C for 120 min. The solution was cooled to room temperature and aged for 24 h. Several precursors were prepared with different sol molarities (0.2, 0.4, 0.6, 0.8, and 1 M). We used the spin-coating technique (Specialty Coating Systems G3P-8 Spin Coater) under $N_2$ gas flow for deposition. All ZnO sols were filtered by using a 0.45-μm filter and then spun on glass

substrates at 1000 rpm for 10 s, followed by 3000 rpm spinning for 20 s. The deposited layer was dried at 200°C in air for 10 min. Spinning and drying steps were repeated several times to obtain an appropriate film thickness (~120 nm). After depositing the last layer, the final film was thermally treated at different sintering temperatures (400, 450, 500, 550, and 600°C) for 1 h in air. ZnO thin films were annealed in FG at 500°C for 30 min. The ZnO film structure was examined by using a Shimadzu (XRD-6000) X-ray diffractometer with CuK$\alpha$ radiation (l = 1.5418 Å). The X-ray tube current and voltage were 30 mA and 40 kV, respectively. The experimental peak positions were compared with the standard JCPDS files and the Miller indices were indexed to the peaks. The surface morphology of the films was studied by atomic force microscopy (AFM Veeco CP-II) in contact mode with Si tips at a scan rate of 1 Hz. A double-beam spectrophotometer (Shimadzu 3150 UV-VIS-NIR) with 0.1 nm resolution was used to measure the transmittance spectra T($\lambda$) at a normal incidence with a wavelength from 200 to 2500 nm.

## 3. Results and discussion

### 3.1. Structural properties

Under the identical conditions, all ZnO thin-film samples were prepared by using the same procedures starting from spinning from ZAD sols of various concentrations (0.2, 0.4, 0.6, 0.8, and 1.0 M), and drying every layer at 200°C in air for ten minutes. Once the last layer, the deposited films were sintered at totally different temperatures (400, 450, 500, 550, and 600°C) for one h in air. The ZnO thin-film thickness that was measured by employing a mechanical stylus profilometer was ~120 nm. The structural properties of the sol-gel-derived ZnO thin films were studied by XRD. The XRD patterns of the ZnO thin films as operate of the sol concentration and heat treatment are shown in Figure one. XRD spectra show that each one films were crystalline with a random orientation. The random orientation, however, contradicts the c-axis-oriented sol-gel ZnO films according by Ohyama et al. [28]. This contradiction presumably results from the distinction within the precursor chemistry and heat-treatment temperature [34]. The most visual phenomenon peaks (100), (002), and (101) correspond to the polygonal shape of hexagonal wurtzite structure of ZnO and matched the space group P63mc (186) well, in line with JCPDS Card No. 89-7102. ZnO films of 0.2, 0.4, and 0.6 M demonstrated a decent crystallinity, whereas the intensity of the three main diffraction peaks was virtually equal and affirms the irregular direction and random orientation, as shown in Figure one (a, b, and c respectively). .

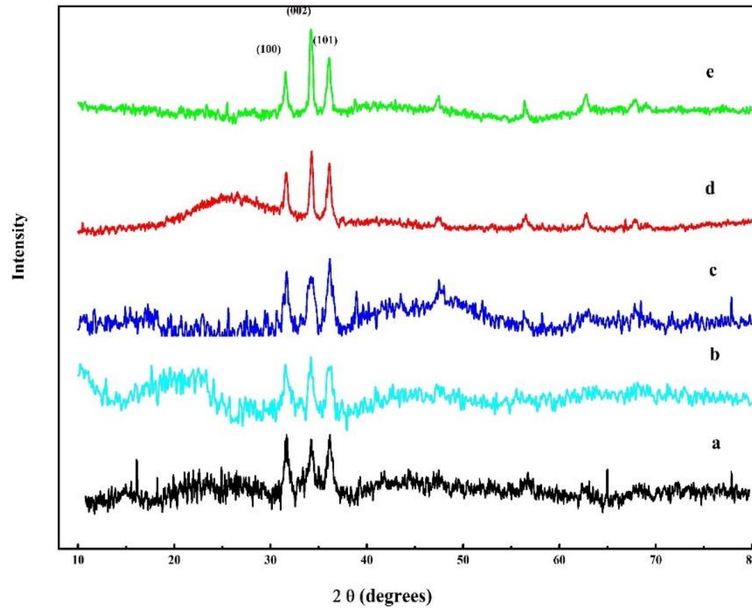


*Fig. 1. XRD patterns of ZnO films of different concentrations, a) 0.2 M, b) 0.4 M, c) 0.6 M sintered at 450°C and 0.4 M ZnO film sintered at d) 500°C and e) 550°C.*

The upper concentrations of ZnO films (0.8 and 1.0 M, not shown here) represent a deficient and poor crystallinity. For the 0.2 and 0.6 M ZnO films, the intensity of the (0 0 2) peak abatements with an increase in Zn concentration, whereas the (1 0 0), (1 0 1), (1 0 2), and (1 1 0) peaks increase gradually. The increase in those peaks intensity indicates an increase in the grain-boundary density for the thin films [29]. The highest degree of orientation along the c-axis (0 0 2), perpendicular to the substrate plane, was observed for the 0.4 M ZnO film

The change in the preferred film orientation was determined quantitatively by calculating the texture coefficient parameter $TC_{(hkl)}$. $TC_{(hkl)}$ in different directions can be estimated by using the following relationship:

$$TC_{(hkl)} = \frac{\frac{I_{(hkl)}}{I_o}}{1/N \sum \frac{I_{(hkl)}}{I_o}} \tag{1}$$

where $I_{(hkl)}$ is the measured intensity of the (hkl) reflection, $I_{o(hkl)}$ represents the standard intensity of the (hkl) reflection from the standard powder pattern diffraction data JCPDS, and N is the number of reflections. As recorded in Table 1, the biggest $TC_{(002)}$ (~2.83) was accomplished from the 0.4 M ZnO film, which confirms the best c-axis growth of the (002) preferred orientation. The degree of c-axis orientation for ZnO thin films is strongly dependent on the initial zinc concentration in solution [30, 31]. The average grain size (δ) along each orientation can be calculated by using the values of the full width at half maximum (FWHM) and the diffraction angle (θ) of each peak from Scherer's formula:

$$\delta = 0.9\ \lambda\ /\text{FWHM}\ \text{Cos}\ (\theta) \tag{2}$$

The lattice strain in the ZnO thin films along the c-pivot upright to the substrate surface can be calculated from:

$$\varepsilon = \frac{c - c_o}{c_o} \times 100 \tag{3}$$

where c denotes the lattice parameter of the hexagonal cell of the deposited ZnO thin films and $c_o$ to the unstrained lattice parameter for bulk ZnO ($c_o$ = 5.2066 Å). The residual stress (σ) in the thin film can be determined from:

$$\sigma = \left(-232.8\,\frac{c - c_o}{c_o}\right) \tag{4}$$

The microstructural parameters (crystallite size, lattice strain, and residual stress) and the cross section lattice parameters of the unit cell (a and c) along the (002) overwhelming orientation for various molar proportions are recorded in Table 1.

*Table 1. Microstructural parameters (crystallite size, lattice strain, and residual stress) and lattice parameters of unit cell (a and c) along (002) predominant orientation for AZO films of different concentrations.*

| Sol concentration (M) | $TC_{(002)}$ | a (Å) | c (Å) | δ (nm) | ε (%) | σ (GPa) |
|---|---|---|---|---|---|---|
| 0.2 | 1.93 | 3.23 | 5.201 | 15.2 | –0.11 | 0.25 |
| 0.4 | 2.83 | 3.21 | 5.203 | 22.4 | –0.069 | 0.16 |
| 0.6 | 2.32 | 3.24 | 5.226 | 19.1 | 0.37 | –0.87 |
| 0.8 | 2.01 | 3.25 | 5.228 | 13.4 | 0.41 | –.96 |
| 1.0 | 0.98 | 3.24 | 5.230 | 12.2 | 0.45 | –1.05 |

The determined grain sizes went somewhere in the range of 12.2 and 22.4 nm. The grain size expanded from 15.2 nm to 22.4 nm when the convergence of the sol expanded from 0.2 to 0.4 M and afterward diminished again to 12.2 nm for 1.0 M. The comparable conduct of crystallite size variety with sol molarity was seen by Benramache et al [32]. They found that the normal grain size expanded to 64 nm when the sol fixation expanded from 0.05 to 0.1 M and subsequently lessened to 36 nm at 0.125 M. They ascribed the enormous crystallite size to the improvement in crystallinity of the ZnO thin films. Zhang [33] found that an expansion in (002) top powers and their grain size demonstrates an improvement in the film crystallinity and an upgrade in the c-pivot direction of the films.

The lattice strain declined in the beginning and afterward increased with an expansion in sol concentration, which shows the presence of a high film tension for sol molarity above 0.4 M. ZnO films of 0.4 M have the biggest crystallite size and the lowest lattice strain as introduced in Figure 2. The negative or positive sign designates a compressive or tensile stress, respectively. Routinely, extrinsic and intrinsic stresses are present together in high-thickness (≥ 300 nm) thin films. Notwithstanding an increase in sol concentricity bringing about an excess in film thickness, all our deposited film thicknesses (~120 nm) were underneath 300 nm. In this way, an extrinsic stress will not be available and the total estimated stress appears to be a prevailing intrinsic stress. All ZnO films, aside from the 0.2 and 0.4 M films, display a compressive stress with a high strain. The calculated values of stress was found to be decreased firstly from 0.25 GPa for 0.2 M to 0.16 GPa for 0.4 M and then increased again with increasing the sol molarity of ZnO films. When the sol molarity exceeds 0.4 M, the value of compressive stress increased again. Snowballing the value of stress may be attributed to weakness of crystallinity that leads to forming the lattice defects and occurring the lattice distortions in the crystal structure [34]. Such behavior was supported by the XRD results that are shown in Figure 1. For the 0.4 M ZnO film, the minimum value of tensile stress (0.16 GPa) follows up on the film and prolongs the lattice constant c (5.203 Å). Nagayasamy et al. [35] reported that the grain size increased and strain decreased by increasing the sol concentration to 0.5 M and then these trends reversed. The variation of (0 0 2) peak power, increases in the beginning and then declines, recording the highest value for 0.4M

ZnO film which proposes that the higher direction of the c-axis plane outcomes from the development of the extra dangled and nearly stress-free film at 0.4 M concentration.

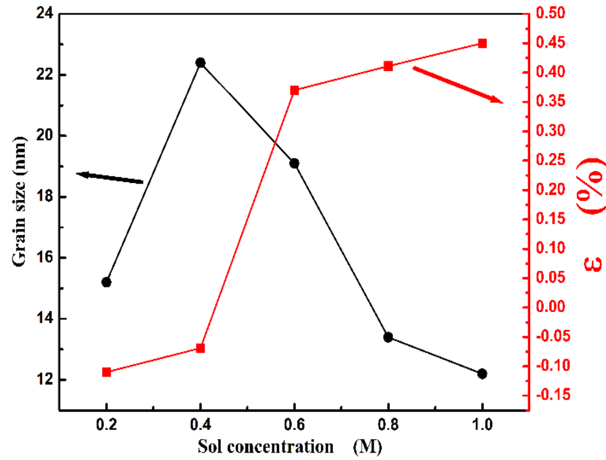


*Fig. 2. Variation of grain size and lattice strain with sol molarity of ZnO thin films.*

Post-heat treatment may be a regular and active way to change inherent deformities and develop crystallinity. To establish the effect of sintering temperature (400–600°C) on the film structure, Figure 1 (d, e) shows XRD examples of the 0.4 M ZnO slim films that were sintered at various temperatures (for example at 500 and 550°C). Compared with the XRD data of the 0.4 M ZnO film that was sintered at 450°C (Figure 1 (b)), the diffraction top power increments with an rise in the temperature of sintering process, which suggests that sintering at a high temperature (500–600°C) improves the crystallization process that resulting in high quality ZnO films. The power of the (002) diffraction peak increases with an increase in the sintering temperature, whereas the other diffraction peaks remain weak, which indicates that at a high temperature, the crystallinity improves with a favored alignment along the *c*-axis vertical to the glass substrate. As a rule, ZnO commonly develops along the c-axis owing to the smallest value of surface energy of the (001) basal plane and its minimum internal stress [36, 37]. ZnO thin films with C-axis preferred orientation have been acquired by utilizing other synthesis procedures, such as rf sputtering [38], chemical deposition [39], and laser ablation [40]. All structural parameters, including the crystallite size, lattice strain, and residual stress and the unit cell parameters (a and c) for the 0.4 M ZnO film that was sintered at diverse temperatures are summarized in Table 2.

*Table 2. Structural parameters (crystallite size, lattice strain, and residual stress) and the lattice parameters of the unit cell (a and c) along a (002) predominant orientation for ZnO films sintered at various temperatures.*

| Sintering temp. (°C) | $TC_{(002)}$ | a (Å) | c (Å) | δ (nm) | ε (%) | σ(GPa) |
|---|---|---|---|---|---|---|
| 400 | 1.48 | 3.21 | 5.2141 | 15.6 | 0.14 | –0.33 |
| 450 | 1.68 | 3.22 | 5.2112 | 19.5 | 0.085 | –0.197 |
| 500 | 2.11 | 3.24 | 5.2021 | 23.2 | –0.078 | 0.18 |
| 550 | 1.51 | 3.23 | 5.2040 | 28.5 | –0.05 | 0.12 |
| 600 | 1.25 | 3.25 | 5.2125 | 24.2 | 0.11 | –0.26 |

The calculated crystallite size increased from 15.6 to 28.9 nm by increasing the sintering temperature from 400 to 600°C. The stress changed from compressive (for samples sintered at 400, 450 and 600°C) and tensile (for samples sintered at 500 and 550°C). The compressive stress varied between –0.33 to –0.42 GPa by increasing the sintering temperature from 400 to 600°C.

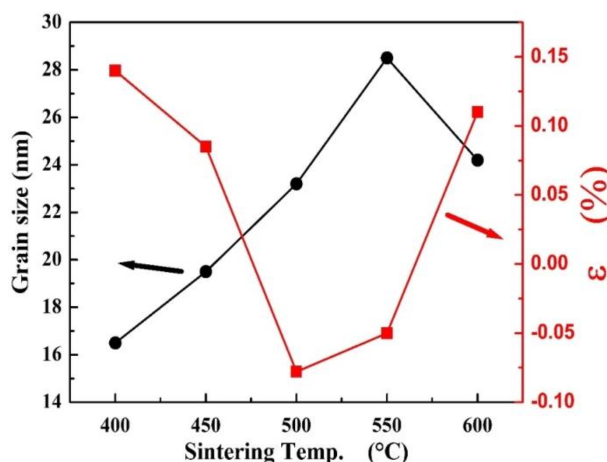


*Fig. 3. Variation of grain size and lattice strain as a function of sintering temperature.*

The tensile stress was 0.18 GPa for film sintered at 500°C and reached a minimum (0.12 GPa) for films sintered at 550°C, which is nearly free of stress. Figure 3 shows the variation of particle size and lattice strain as a function of sintering temperature. As the sintering temperature increases, the crystallite size increases, whereas the lattice strain decreases. Jian-Ping et al. reported that the lattice strain of ZnO thin films decreased with an increase in annealing temperature up to 700°C and then increased. They attributed this behavior to various types of film defects [41]. A similar behavior for ZnO thin-film strain was observed by Lu et al. [42].

The surface morphology of ZnO films of different sol concentrations was investigated by AFM as shown in Figure 4 (a, b and c). The solution concentration was increased and an abrupt change in the surface morphology of the films was visible from the micrographs. The surface consisted of irregular and disordered granular particles with a highly porous structure as seen from the image of the 0.2 M ZnO films (Figure 4(a)). This disorder explains the weak crystalline orientation along the (002) direction shown in the XRD spectrum. ZnO thin films at 0.4 M have a more compact, uniform, and dense film with a smooth surface coverage of planar grains with irregular shapes on a predominantly porous structure (Figure 4(b)). However, films that were deposited at a higher concentration of 0.8 M had a compact surface but a high roughness and larger peak to valley (Figure 4(c)).

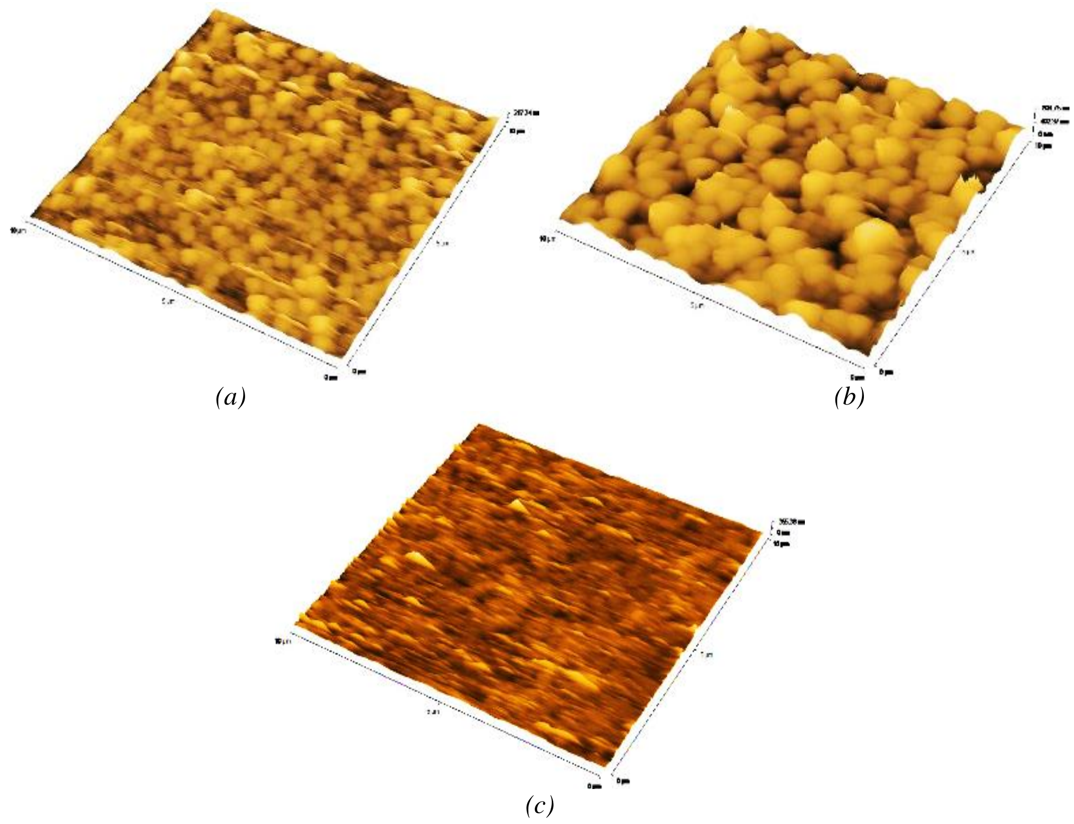

*Fig. 4. AFM images of ZnO films of different concentrations, a) 0.2 M, b) 0.4 M, c) 0.6 M sintered at 450°C.*

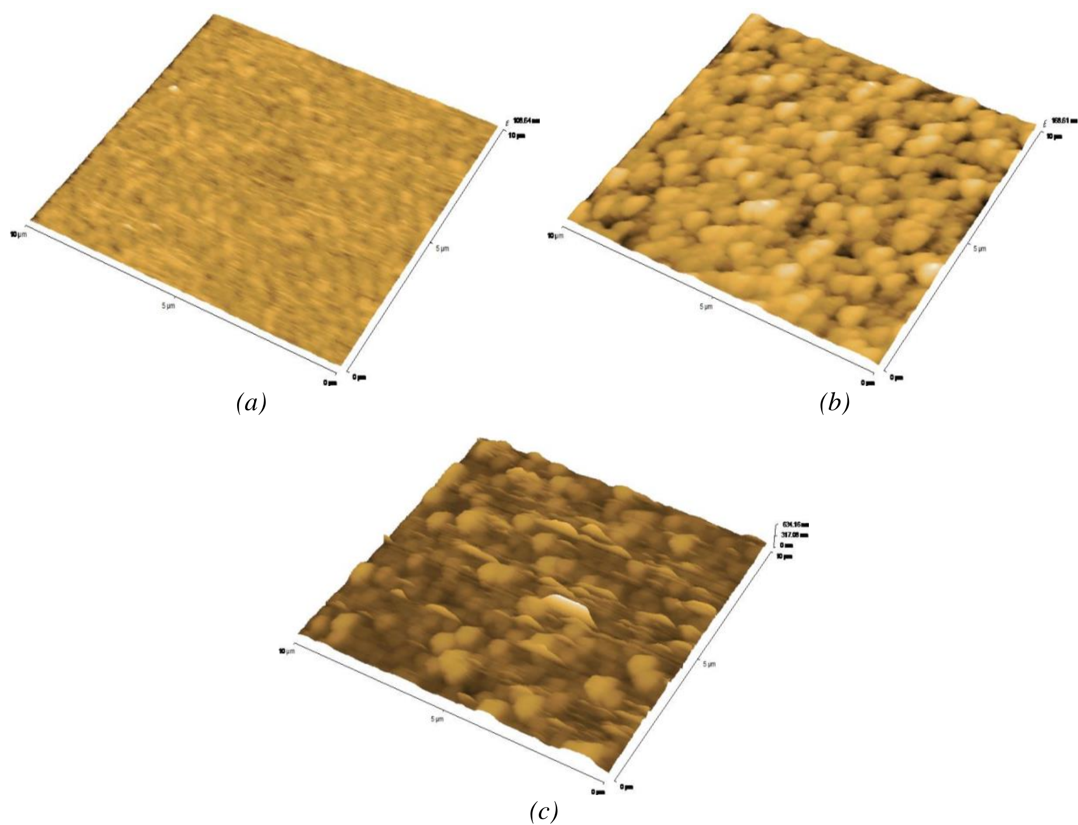

*Fig. 5. AFM images of 0.4 M ZnO films sintered at a) 500, b) 550, and c) 600°C.*

Figure 5 (a, b and c) represent the surface morphology of 0.4 M ZnO films that were sintered in air for 1 h at different temperatures (450, 550, and 600°C), respectively. The ZnO film that was sintered at 450°C exhibited a smooth surface that had a small grain size, as shown in Figure 5 (a). An increase in sintering temperature to 550°C increased the grain size of the film, whereas a temperature up to 600°C resulted in a larger grain size and high roughness, as shown by Figure 5 (b and c), respectively.

### 3.2. Optical properties

The optical transmission spectra of ZnO thin films were measured from 200 to 2200 nm. The transmittance spectra of ZnO films of different sol concentrations (0.2, 0.4, 0.6, 0.8, and 1.0 M), sintered at 450°C for 1 h in air followed by annealing at 500°C for 30 min in FG ambient are recorded in Figure 6. All ZnO films of different concentrations exhibit a high transparency (near 90%) in the infrared and visible-light range, whereas in the ultraviolet region, the transmittance decreased sharply because of the forbidden energy gap of the ZnO films [43]. Such behavior indicates the stoichiometric and homogeneous structure of the studied samples [44].

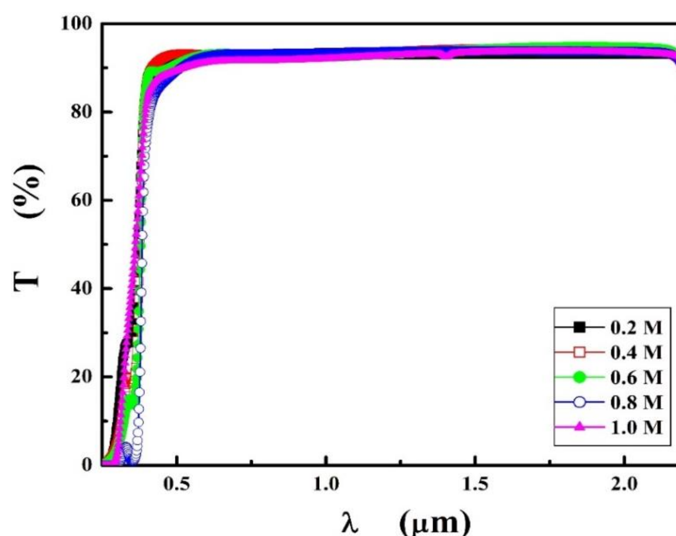


*Fig. 6. Transmittance spectra of ZnO films of different sol concentrations (0.2, 0.4, 0.6, 0.8, and 1.0 M), sintered at 450 ℃ for 1 h in air followed by further annealing at 500 ℃ for 30 min in FG ambient.*

The optical absorption edge was analyzed from:

$$\alpha h v = A(h v - E_g)^r \quad (5)$$

where hv is the photon energy, Eg is the optical band gap, and A is a constant. The exponent (r) is used to determine the type of electronic transition. By plotting Ln (α) versus hv (not shown here) the slope was found to be r = ½, which indicates a direct band-gap transition. By substituting r = 1/2 and squaring the above equation:

$$(\alpha h v)^2 = A(h v - E g) \quad (6)$$

By plotting $(\alpha h v)^2$ versus hv, Eg could be determined from the slope and the intercept of the straight line. In Figure 7, $(\alpha h\nu)^2$ vs hv was plotted for ZnO films of different sol concentrations.

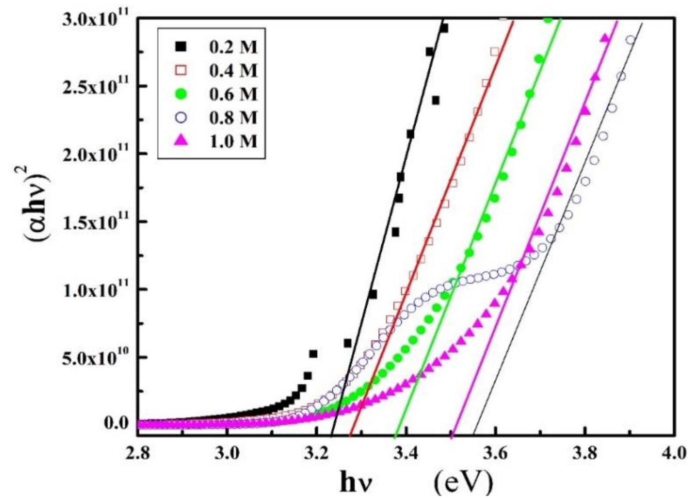


*Fig. 7. $(\alpha h\nu)^2$ vs hν for ZnO films of different sol concentrations.*

The variation in sol concentration changes the optical Eg. The obtained Eg increased from 3.24 eV to 3.55 eV when the solution molarity increased from 0.2 to 0.8 M, respectively. Eg decreased to 3.50 eV for the 1.0 M ZnO film. Efafi et al. [45] found that an increase in sol concentration of the AZO films lead to a decrease in the optical transmission in the visible region and a red shift in the transmission spectrum by reducing the energy band gap to 3.28 eV. Benramache et al. [32] found that an increase in the precursor molarity from 0.05 to 0.1 M increased the Eg from 3.08 to 3.37 eV.

The effect of sintering temperature on the optical transmittance and Eg values of ZnO thin films was studied. The transmittance spectra of ZnO films sintered at different temperatures were measured and are presented in Figure 8. The high value of transmission (~90%) was observed in the infrared and visible wavelength range for all samples. However, ZnO films sintered at 550 and 600°C exhibit a low value of transmission (~80%). In the ultra-violate region, the transmittance of all ZnO films decreases sharply because of the band-gap absorption.

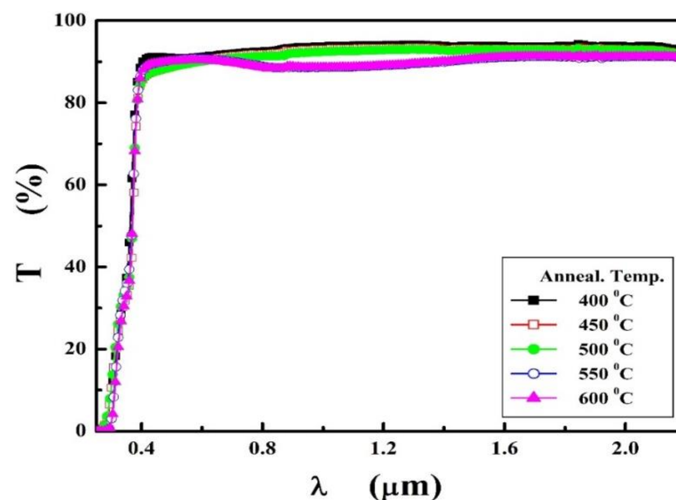


*Fig. 8. Transmittance spectra of ZnO films sintered at different sintering temperatures.*

The absorption edge of ZnO films sintered at 550 and 600°C shifted to a longer wavelength. The linear relationship between $(\alpha h\nu)^2$ and the photon energy hν, as shown in Figure 9, was used to estimate Eg.

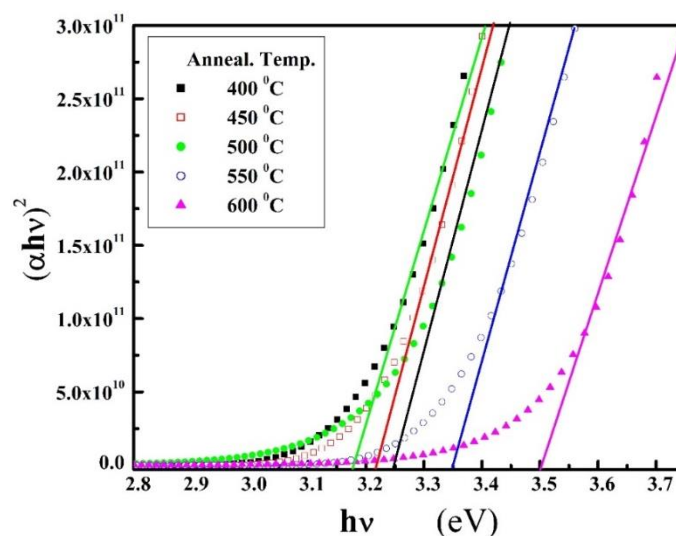


*Fig. 9. $(\alpha h\nu)^2$ vs photon energy hν for 0.4 M ZnO films sintered at different temperatures.*

Eg was 3.17 eV for ZnO film sintered at 400°C and increased with sintering temperature to 3.50 eV for film sintered at 600°C. The difference in atomic structure between the inside grain and at the grain boundaries caused an excess of free carrier density and potential barrier at the boundaries, which formed an electric field that increased the band gap [46, 47]. Eg could be related to the film stress. According to Pankove, the Eg value is dependent on the interatomic spacing of semiconductors, which is caused by changes in the film stress [48]. Ghosh and Srikant reported that the Eg increases with an increase in compressive strain/ tensile stress along the c-axis but decreases with an increase in tensile strain/compressive stress [49]. The increase in Eg could be attributed to the evaporation of impurity ions (OH-ions), which reduces Eg [50]. The increase in Eg may occur because of the band bending effect (Urbach energy) within the ZnO films. Such a variation of Eg with heat treatment was observed for Al-doped ZnO films by Malek et al. [51]. They discussed their results based on the intrinsic and extrinsic defects of the film and the Burstein–Moss effect.

### 3.3. Electrical properties

The electrical sheet resistance ($R_{\square}$) of ZnO thin films that were deposited from a ZAD sol of different concentrations (0.2–1.0 M) and sintered at 450°C in air for 1 h was measured by using the four-probe technique. By using the values of $R_{\square}$ and the film thicknesses (d), the electrical resistivity (ρ) was calculated. The electrical resistivity of the ZnO film decreases with an increase in the sol concentration from 0.2 to 0.4 M and then increased with an increase in sol concentration, as shown in Figure 10. The lowest electrical resistivity, $12.5 \times 10^2$ Ω.cm was obtained with 0.4 M ZnO films. To establish the effect of heat treatment, 0.4 M ZnO thin films were prepared and sintered at different sintering temperatures (400–600°C). As expected, the electrical resistivity of the ZnO films decreased with an increase in sintering temperature. The electrical resistivity decreased to 250 Ω.cm when the sintering temperature increased to 550°C in air. The electrical resistivity of ZnO films decreased after annealing at 500°C in FG for 30 min, by one to two orders of magnitude. Figure 11 shows the variation in electrical resistivity with sintering temperature before and after annealing in FG.

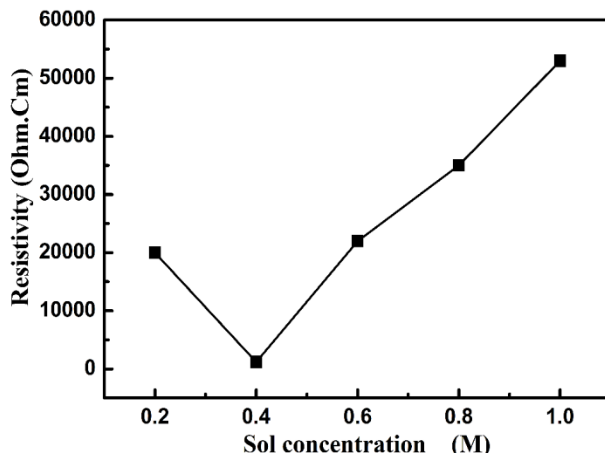


*Fig. 10. Dependence of electrical resistivity of ZnO film on the sol concentration.*

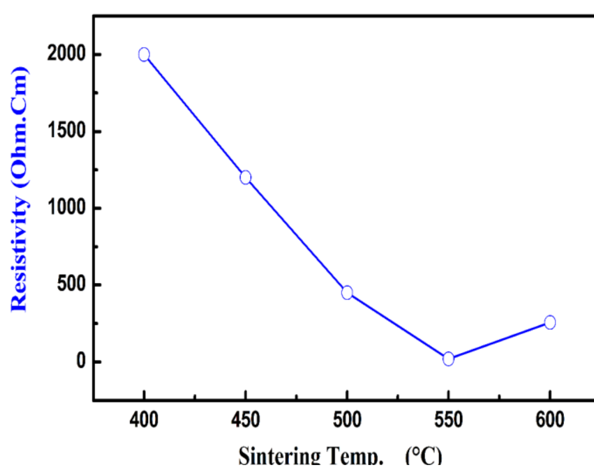


*Fig. 11. Dependence of electrical resistivity of 0.4 M ZnO film on the sintering temperature.*

The lowest electrical resistivity was 22.0 Ω.cm after sintering of the 0.4 M ZnO film at 550°C for 1 h followed by annealing at 500°C in FG for 30 min. The decrease in electrical resistivity by annealing in FG could be attributed to the reaction of H atoms of FG with O atoms of the ZnO film that leaves O vacancies and free electrons, which increases the electrical conductivity. However, the resistivity of all annealed ZnO films remains higher than the published values for ZnO films prepared by other techniques. In literature, the electrical resistivity for the ZnO thin films ranged from 0.1 to 100 Ω.cm and such low values were related to an increase in (002) orientation degree of its hexagonal wurtzite crystal structure [52]. Nevárez et al. found that the lowest electrical resistivity of 7.1 Ω.cm for a ZnO film was prepared with isopropanol after annealing at 400°C and they attributed this result to the high number of oxygen vacancies [53].

### 3.4. Correlation between microstructure, optical and electrical properties

Figure 12 shows the influence of sol concentration on the microstructural (grain size), optical (Eg), and electrical (resistivity) parameters. By varying the sol concentration, the grain size increases to 0.4 M and then decreases with an increase in sol molarity. The opposite behavior was observed for the electrical resistivity, which decreased initially and then increased beyond 0.4 M. The largest grain size (22.4 nm) that was associated with the lowest electrical resistivity (1200 Ω. Cm) was achieved at a 0.4 M sol concentration. The Eg increased to 3.55 eV with an increase in the sol molarity to 0.8 M and suddenly decreased to 3.5 eV at 1.0 M. For 0.4 M ZnO thin films, the sintering temperatures affected the structural, optical, and electrical parameters as shown in

Figure 13. The sample sintered at 550°C had the largest grain size of ~28 nm and was associated with the lowest electrical resistivity. An inverse relationship existed between grain size and electrical resistivity. An increase in particle size may decrease grain-boundary scattering and thus, the electrical resistivity decreased.

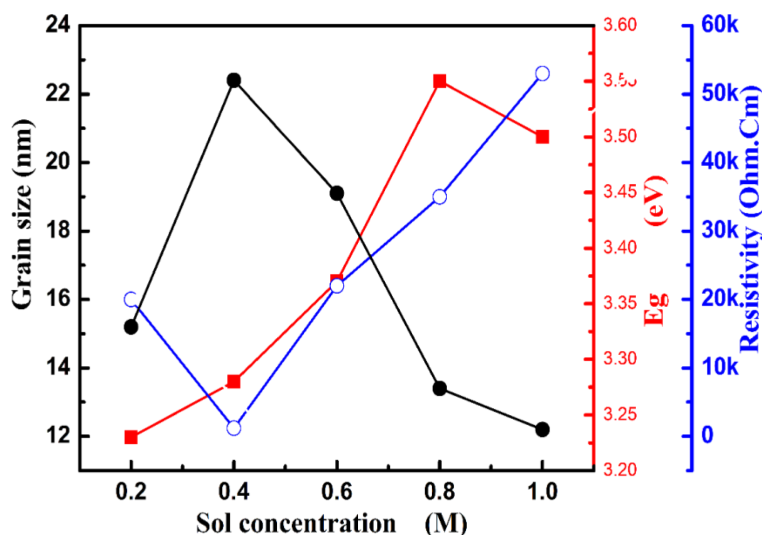


*Fig. 12. Variation of grain size, band-gap energy (Eg), and electrical resistivity with sol concentration.*

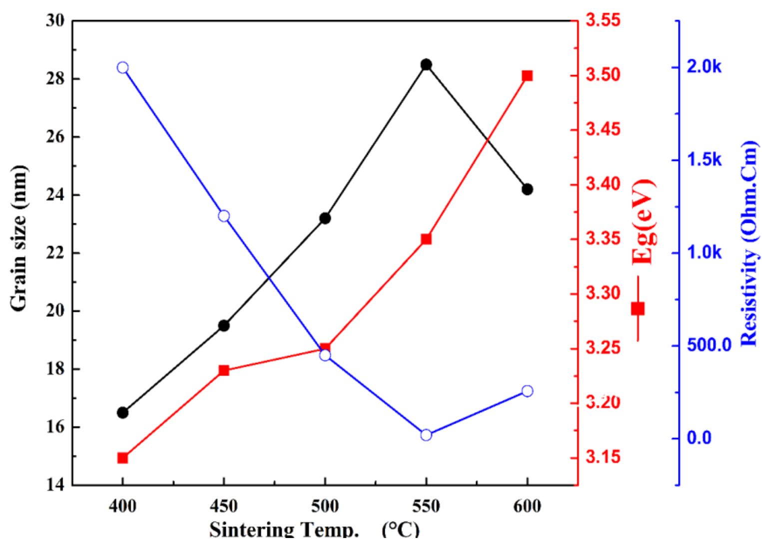


*Fig. 13. Variation of grain size, band-gap energy (Eg), and electrical resistivity of 0.4 M ZnO films with sintering temperature.*

## 5. Conclusions

Transparent conductive ZnO thin films were deposited on glass substrates by using sol–gel spin coating. The effect of sol concentration and sintering temperature on the structural, optical, and electrical properties was investigated. The relationship between the crystallite size, stress and strain, optical gap energy, and electrical resistivity through the variation of precursor molarity and heat treatment was discussed. From our results, we conclude the following:

(1) XRD patterns showed a polycrystallinity of hexagonal wurtzite phase with random orientation for all ZnO thin films. The film obtained with 0.4 M ZnO had a higher (002)

diffraction peak intensity indicating the nanocrystallinity of the films with a desired direction to the c-axis upright to the surface of substrate.

(2) The grain size increased with molarity up to 0.4 M and beyond that point, it decreased. For the 0.4 M film, the crystallite size enlarged with an increase in sintering temperature. Its value grows from 1506 to 28.9 nm by raising the curing temperature from 400 to 600°C.

(3) The value of Eg expanded from 3.24 to 3.55 eV with growth in precursor molarity from 0.2 to 0.8 M. An increase in curing temperature from 400 to 600°C amplified the Eg from 3.17 to 3.5 eV for the 0.4 M ZnO films.

(4) The lowest electrical resistivity was of 22.0 Ω.cm, which was achieved after sintering the 0.4 M ZnO film at 550°C for 1 h supervened by annealing at 500°C in FG for 30 min.

(5) Based on the variation of sol concentration and sintering temperature the structural, electrical, and optical properties were correlated. It was established that the grain size of the ZnO films is affected mainly by the lattice stress and strain, whereas it has a strong effect on the Eg and the electrical resistivity.

## Acknowledgments

The authors acknowledge the Deanship of Scientific Research at King Faisal University for the financial support under Nasher Track (grant No. 186265)

## References

[1] Benramache S, Arif A, Belahssen O, et al. (2013), Journal of Nanostructure in Chemistry, 3(80): 1; https://doi.org/10.1186/2193-8865-3-80

[2] C. Klingshirm, (1975) Phys. Status Solidi (b) 71: 547; https://doi.org/10.1002/pssb.2220710216

[3] Benramache S, Rahal A, Benhaoua B. (2014), Optik, 125(2): 663; https://doi.org/10.1016/j.ijleo.2013.07.085

[4] Benzarouk H, Drici A, Mekhnache M, et al. (2012), Superlattices and Microstructures, 52(3): 594; https://doi.org/10.1016/j.spmi.2012.06.007

[5] P. F. Carcia, R. S. McLean, M. H. Reilly, and G. Nunes, (2003) Appl. Phys. Lett. 82: 1117; https://doi.org/10.1063/1.1553997

[6] M. Tomar, V. Gupta, K. Sreenivas, A. Mansingh, (2005) IEEE Trans. Devices Mater. Reliab. 5: 494; https://doi.org/10.1109/TDMR.2005.853453

[7] V. Srikant, S. Valter, R. David, (1995) J. Am. Ceram. Soc. 78: 1931; https://doi.org/10.1111/j.1151-2916.1995.tb08912.x

[8] S. P Singh, S. K. Arya, P. Pandey, B. D. Malhotra, S. Saha, K. Sreenivas, and V. Gupta, (2007) Appl. Phys. Lett. 91: 063901; https://doi.org/10.1063/1.2768302

[9] C. S. Lao, Q. Kuang, Z. L. Wang, M. C. Park, and Y. Deng, (2007) Appl. Phys. Lett. 90: 262107; https://doi.org/10.1063/1.2748097

[10] R. Martins, E. Fortunato, P. Nunes, I. Ferreira, A. Marques, M. Bender, N. Katsarakis, V. Cimalla, and G. Kiriakidis, (2004) J. Appl. Phys. 96: 1398; https://doi.org/10.1063/1.1765864

[11] H.G. Swamy, P.J. Reddy, (1990) Semicond. Sci. Technol. 5: 980; https://doi.org/10.1088/0268-1242/5/9/009

[12] S.S. Lin, J.L. Huang, (2004) Surf. Coat. Technol. 185: 222; https://doi.org/10.1016/j.surfcoat.2003.11.014

[13] S.K. Ghandhi, R.J. field, J.R. Shealy, (1980) Appl. Phys. Lett. 37: 449; https://doi.org/10.1063/1.91960

[14] M.F. Ogawz, Y. Naysume, T. Hirayama, (1990) J. Mater. Sci. Lett. 9: 1351; https://doi.org/10.1007/BF00726543

[15] O. Pagni, N.N. Somhlahlo, C. Weichsel, A.W.R. Leitch, (2006) Physica B 376- 377: 749; https://doi.org/10.1016/j.physb.2005.12.187

[16] E. R. Shaaban, (2006) ) Physica B 373: 211; https://doi.org/10.1016/j.physb.2005.11.145
[17] J.H. Lee, B.O. Park, (2003) Thin Solid Films 426: 94; https://doi.org/10.1016/S0040-6090(03)00014-2
[18] Hadis Morkoç and Ümit ÖzgÜr, (2009) Zinc Oxide: Fundamentals, Materials and Device Technology, WILEY-VCH Verlag GmbH & Co. KGaA, Weinheim ISBN: 978-3-527-40813-9; https://doi.org/10.1002/9783527623945
[19] Ya Qi Hou, Da Ming Zhuang, Gong Zhang, Ming Zhao, Min-Sheng Wu., (2003) Applied Surface Science 218: 98-106; https://doi.org/10.1016/S0169-4332(03)00569-5
[20] Mehmet Tumerkan Kesim, Caner Durucan., (2013), Thin Solid Films 545: 56-63; https://doi.org/10.1016/j.tsf.2013.07.031
[21] Kewei Sun, Wancheng Zhou, Xiufeng Tang, Zhibin Huang, Fa Luo, Dongmei Zhu., (2012), Surface and Coatings Technology 206: 4095-4098; https://doi.org/10.1016/j.surfcoat.2012.04.001
[22] Zendehnama, M. Mirzaeec, S. Miri., (2013); Applied Surface Science 270: 163-168; https://doi.org/10.1016/j.apsusc.2012.12.154
[23] Davood Raoufi and Taha Raoufi., (2009), Journal of Applied Surface Science 255: 5817-5824; https://doi.org/10.1016/j.apsusc.2009.01.010
[24] Cui M.L, X.M. Wu, L.J. Zhuge, Y.D. Meng.,(2007) Effects of annealing temperature on the structure and photoluminescence properties of ZnO films. 81: 899-903; https://doi.org/10.1016/j.vacuum.2006.10.011
[25] Habibi M.H, M.K. Sardashti., (2008), Journal of Iranian Chemistry Society 5: 603-609; https://doi.org/10.1007/BF03246140
[26] Nanda Shakti and P.S Gupta., (2010), Journal of Applied Physics Research 2: 19-28; https://doi.org/10.5539/apr.v2n1p19
[27] H. H. Somaily, Kh. S. Shaaban, Sayed A. Makhlouf, H. Algarni, H. H. Hegazy, E. A. Wahab, ER Shaaban, (2021) J Inorg Organomet Polym Mater. 31, 138; https://doi.org/10.1007/s10904-020-01650-2
[28] M. Ohyama, H. Kozuka, T. Yoko, (1998) J. Am. Ceram. Soc. 81: 1622; https://doi.org/10.1111/j.1151-2916.1998.tb02524.x
[29] M. Oztas, M. Bedir, S. Sur, and Z. Öztürk, (2012) "Influence of an aqueous/ethanolic solution on the structural and electrical properties of polycrystalline ZnS films," Chalcogenide Letters, vol. 9, no. 6. pp. 249-256.
[30] S. O'Brien, L. H. K. Koh, and G. M. Crean, (2008), Thin Solid Films, vol. 516, no.7: 1391-1395; https://doi.org/10.1016/j.tsf.2007.03.160
[31] V. R. Shinde, T. P. Gujar, and C. D. Lokhande, (2007), Sensors Actuators, B Chem., vol. 120, no. 2: 551-559; https://doi.org/10.1016/j.snb.2006.03.007
[32] S. Benramache, O. Belahssen, A. Guettaf, and A. Arif, (2014), Journal of Semiconductors Vol. 35, No. 4: 042001; https://doi.org/10.1088/1674-4926/35/4/042001
[33] Zhang C. (2010), J Phys Chem Solids, 71(2): 364; https://doi.org/10.1016/j.jpcs.2010.01.001
[34] S. Y. Kuo et al., (2006), J. Cryst. Growth, vol. 287, no. 1: 78-84; https://doi.org/10.1016/j.jcrysgro.2005.10.047
[35] N. Nagayasamy, S. Gandhimathination, and V. Veerasamy, (2013), Open J. Met., vol. 3, no. 2: 8-11; https://doi.org/10.4236/ojmetal.2013.32A2002
[36] Zhang H Z, Sun X C, Wang R M and Yu D P (2004) J. Cryst. Growth 269: 464; https://doi.org/10.1016/j.jcrysgro.2004.05.078
[37] D. Bao, H. Gu, A. Kuang, (1998) Thin Solid Films 312: 37; https://doi.org/10.1016/S0040-6090(97)00302-7
[38] E. R. Shaaban, I. S. Yahia, M. Fadel (2009) Journal of alloys and compounds 469, 427: https://doi.org/10.1016/j.jallcom.2008.01.155
[39] Y. Kashiwaba, F. Katahira, K. Haga, T. Sekiguchi, H. Watanabe, (2004) J. Cryst. Growth 221: 431; https://doi.org/10.1016/S0022-0248(00)00729-6
[40] Y.R. Ryu, W.J. Kim, H.W. White, (2000) J. Cryst. Growth 219: 419; https://doi.org/10.1016/S0022-0248(00)00731-4
[41] XU Jian-Ping, SHI Shao-Bo, LI Lan, ZHANG Xiao-Song, WANG Ya-Xin, CHEN Xi-Ming, (2010) CHIN. PHYS. LETT. Vol. 27, No. 4: 047803; https://doi.org/10.1088/0256-307X/27/4/047803

[42] Lu J G et al (2006) J. Appl. Phys. 100: 073714; https://doi.org/10.1063/1.2357638
[43] G. Harbeke, (1985) Polycrystalline Semiconductors: Physical Properties and Applications, Springer-Verlag, Berlin; https://doi.org/10.1007/978-3-642-82441-8
[44] E.K. Kim, S. Kim, (2007) Superlattices Microstruct. 42: 343; https://doi.org/10.1016/j.spmi.2007.04.012
[45] B. Efafi, S. S. Mousavi, M. H. M. Ara, B. Ghafari, and H. R. Mazandarani, (2017), Mater. Lett., vol. 195: 52-54; https://doi.org/10.1016/j.matlet.2017.02.079
[46] Y.-S. Kim, W.-P. Tai, and S.-J. Shu, (2005), Thin Solid Films, vol. 491, no. 1-2: 153-160; https://doi.org/10.1016/j.tsf.2005.06.013
[47] J. Rodríguez-Báez, A. Maldonado, G. Torres-Delgado, R. Castanedo-Pérez, and M. D. L. L. Olvera, (2006), Mater. Lett., vol. 60, no. 13-14: 1594-1598; https://doi.org/10.1016/j.matlet.2005.11.077
[48] J. I. Pankove and D. A. Kiewit, (1972), J. Electrochem. Soc., vol. 119, no. 5: 156C; https://doi.org/10.1149/1.2404256
[49] R. Ghosh, D. Basak, and S. Fujihara, (2004), J. Appl. Phys., vol. 96, no. 5: 2689-2692; https://doi.org/10.1063/1.1769598
[50] F.I. Ezema, U. O. A. Nwankwo, (2010) "Effect of annealing temperature on the structural and optical properties of zinc oxide (ZnO) nanocrystals prepared by sol gel," Dig. J. Nanomater. Biostructures, vol. 5 no 4: 981-988.
[51] M. F. Malek et al., (2015), J. Lumin., vol. 160: 165-175; https://doi.org/10.1016/j.jlumin.2014.12.003
[52] Lee JH, Ko KH, Park BO. (2003), Journal of Crystal Growth. 247(1-2):119-125; https://doi.org/10.1016/S0022-0248(02)01907-3
[53] Gonzalo Alonso Velázquez-Nevárez, Jorge Roberto Vargas-García, Jorge Aguilar-Hernández, Oscar Edgardo Vega-Becerra, Fei Chen, Qiang Shen, Lianmeng Zhang, (2016) Materials Research. 19(Suppl. 1): 113-117; https://doi.org/10.1590/1980-5373-mr-2016-0808

.